Electronic Structure and Localized States in Amorphous Si and Hydrogenated Amorphous Si

Journal:	*Physical Chemistry Chemical Physics*
Manuscript ID	CP-ART-02-2019-001121.R2
Article Type:	Paper
Date Submitted by the Author:	30-May-2019
Complete List of Authors:	Vatan Meidanshahi, Reza; Arizona State University, School of Electrical, Computer and Energy Engineering Bowden, Stuart; Arizona State University Goodnick, Stephen; Arizona State University

Journal Name

ARTICLE TYPE

Cite this: DOI: 00.0000/xxxxxxxxxx

Electronic Structure and Localized States in Amorphous Si and Hydrogenated Amorphous Si†

Reza Vatan Meidanshahi, Stuart Bowden, and Stephen M. Goodnick

Received Date
Accepted Date

DOI: 00.0000/xxxxxxxxxx

Hydrogen incorporation in the fabrication of amorphous Si (a-Si) plays an important role in improving its electronic and optical properties. An important question is how H interacts with the a-Si atomic network, and consequently affects the electronic properties of a-Si. The common assumption is that the role of H is to passivate the dangling bonds (DBs) of the a-Si structure, which subsequently leads to a reduction in the density of midgap sates and localized states within the mobility gap. In the present work, we first employ a combined molecular dynamic (MD) and density functional theory (DFT) method to create stable configurations of a-Si:H, and then analyze the atomic and electronic structure to investigate which structural defects interact with H, and how the electronic structure changes with H addition. We show that in contrast with the simple dangling bond picture, atoms bonded by highly strained bonds (SBs) are significantly affected by the addition of H, in terms of the lowest energy configuration, with similar if not greater importance to that of dangling bonds in passivating a-Si. We find that H atoms decrease the density of mid-gap states of a-Si by bonding to the Si atoms with SBs. Our results also indicate that Si atoms with SBs creates highly localized orbitals in the mobility gap of a-Si and a-Si:H, and the bonding of H atoms to them can significantly decrease the degree of orbital localization. The results demonstrate the beneficial effects of hydrogenation of a-Si in terms of reducing the overall strain energy of the a-Si network, with commensurate reduction of mid-gap states and orbital localization.

Introduction

Amorphous silicon (a-Si) has been utilized in many material technologies such as solar cells, thin film transistors, LCD, photosensors, and photoreceptors [1–6]. It is generally accepted from experimental and theoretical studies that most of the optical and electrical properties of a-Si, including absorption, photodegradation, and charge transport, are strongly affected by the density of mid-gap and localized states in the mobility gap of a-Si, which result from the existence of microscopic structural disorder and defects [7–9]. Dangling bonds are usually believed to be associated with mid-gap and highly localized states in the gap and band tails, and contribute strongly to the optical and electrical properties of a-Si [10–14]. However, there are indications that other metastable and likely less localized structural defects (strained bonds and floating bonds) may also contribute [7,15–19]. Since large amounts of H are usually used to saturate dangling bonds as major defects in an a-Si structure and also since H atoms are able to move in the Si matrix [20,21], the interaction of H with these metastable defects is also a matter of importance in determining the quality of a-Si:H films [22–28]. Different possible interactions of H atoms with these metastable structural defects may result in different atomic configurations, and consequently different properties [24,29].

Amorphous silicon and its hydrogenated forms have been extensively studied both experimentally and theoretically for decades. Efforts aimed at modifying and improving the properties of these materials have been ongoing over many years. In the electronics and optoelectronics fields, theoretical and computational studies have strived to provide new insights into the details of the atomic and electronic structure of these materials, for the device applications of a-Si and a-Si:H. A number of theoretical studies have been reported on generating realistic atomic structures of a-Si and a-Si:H with different methods such as information-based approaches [30], machine learning [31,32], force-enhanced atomic refinement [33,34], DFT [35,36], MD [37,38], nearly hyperuniform network [39] and Wooten-Winer-Weaire [40] methods. Other studies have focused on electronic structure related properties such as the vibrational frequency [41], optical absorption [38,42], optical and mobility gap [43,44] and the relation between atomic and electronic structure [15,17,19,45,46]. However, there are relatively a few studies regarding the interaction of H atoms with different structural defects in a-Si.

Several experimental, theoretical and computational studies

Arizona State University, School of Electrical, Computer and Energy Engineering, Tempe, AZ, 85281, USA; E-mail: rvatanme@asu.edu

†*Electronic supplementary information (SI) available. See DOI: 00.0000/xxxxxxxxxx*

have been reported on the role of H bonding configurations on the properties of a-Si:H beyond the simple interaction of H with DBs. A considerable number of these studies are devoted to the H-assisted Staebler-Wronski effect (SWE) mechanism, which is the photo-degradation of a-Si:H under prolonged exposure to intense light. The proposed models consider the light-induced conversion of some of the weakest Si-Si bonds to dangling bond metastable defects which is strongly accelerated by creating specific forms of H bonding configurations in the transition states or intermediates[23,47–51]. Some other studies have taken into account the effect of the H bonding configuration on the H motion or diffusion in the a-Si network[27]. The main observation is that by assisting some H bonding configurations, H can proceed with an energy barrier much less than that of simple dissociating a Si-H bond. In other works, the mechanism of hydrogen-induced crystallization or disorder-to-order structural transitions in a-Si has been proposed by the configurations resulting from the interaction of H atoms with Si-Si strained bonds[26,52–56]. In contrast to the aforementioned works, to the best of our knowledge, we are not aware of any direct simulation of the variation of a-Si:H electronic structure due to the different interactions of H with metastable defects beyond those of dangling bonds.

In the present work, we report a combined MD/DFT method to create low defect and stable configurations of a-Si:H. The procedure consists of adding hydrogen atoms to a fully optimized a-Si supercell obtained from MD-DFT methods, in which fully optimized DFT calculations were performed on many possible configurations after each H atom addition. The optimized configurations obtained from DFT with the lowest energy were then taken as the most stable configurations, which may or may not be physically realizable with the insertion of H experimentally due to kinetic barriers at a given temperature. Using this method, we generated many stable configurations which differ in H concentration (1-3%) and H position to investigate the effect of the hydrogen addition and H bonding configuration on the atomic and electronic structure of a-Si. This method enables us to investigate which structural defects are more sensitive to the addition of H and which part of electronic structure of a-Si more affected due by this addition.

Methods

Technical Details

We use a melting and quenching approach for generating a structural model of a-Si, as the starting atomic structure for the DFT calculations. The LAMMPS molecular dynamic code[57] is used for simulating the melting and quenching process. In the MD simulation, the Tersoff interatomic potential[58] was employed for describing Si atom interactions, with a cut-off radii of 2.7 Å (taper) and 3.0 Å (maximum); this potential has been widely used for generating Si based structures[59]. Full ion relaxation of the resulting structure from the MD simulation was performed at the DFT-level as implemented in the Quantum Espresso 5.2.1 software package[60]. The three-body dispersion correction was used in all DFT simulations. The BFGS quasi-Newton algorithm, based on the trust radius procedure, was used as the optimization algorithm to find the relaxed structure. The structural analysis of the final a-Si structure was performed using the ISAACS program[61].

Both ionic relaxation and electronic structure calculations was performed using the Becke-Lee Yang-Parr (BLYP) exchange-correlation functional[62,63]. The core and valence electron interactions were described by the Norm-Conserving Pseudopotential function. Unless otherwise stated, an energy cutoff of 12 Ry was employed for the plane-wave basis set and an $4\times4\times4$ k-point mesh was used, with the Monkhorst-Pack grids method for the Brillouin-zone sampling in all the calculations. A Gaussian smearing and fixed method was applied to determine the band occupations and electronic density of states in the case of having odd and even number of H atoms in the supercells, respectively.

Generation of the a-Si and a-Si:H Structures

Molecular dynamics simulations in conjunction with DFT calculations have been demonstrated to yield amorphous material structures whose properties are commensurate with experimental results[64–67]. Therefore, we initially carried out MD simulations to generate a general form of the a-Si structure, and then relaxed the structure using a DFT calculation to obtain an experimentally compatible structures.

MD simulation of the melting and quenching process was carried out on a crystalline Si structure in order to create an a-Si supercell containing 216 Si atoms (a-Si216) with three dimensional (3D) periodic boundary conditions. An initial atomic structure of crystalline Si with a lattice constant of $a_0 = 5.46$ Å was constructed using a cubic supercell with the dimension of $a = b = c = 3a_0$, which was periodically repeated in 3D space to generate an infinite network of atoms. a_0 was chosen in such a way that the mass density of our supercell is equal the mass density of a-Si measured by experiments[68,69]. Then, we carried out a simulated melting process at 3000 K for 10 ps with a fixed volume and temperature ensemble (NVT). A simulation time step of 0.1 fs was used. The structure obtained from the 10 ps melting was consequently quenched to 800 K, with a cooling rate of 6×10^{12} K/s, as used in previous studies[42,43,66,67,70]. For reducing the excess energy of a-Si, we increased the temperature from 800 K to 1600 K, and then quenched it to 300 K with the same quenching rate as before. After quenching, the a-Si structure was annealed for 25 ps at 300 K. Finally, the structure was fully optimized using a DFT relaxation calculation.

We found six dangling bonds (DBs) and no floating bonds (FBs) per supercell, with an assumed Si-Si bond length cutoff of 2.58 Å, which is 10% longer than the experimental Si-Si bond length (2.35 Å). Dangling (floating) bonds are missing (extra) chemical bonds of a Si atom from ideally four chemical bounds. The average Si-Si bond length in the supercell is 2.362 Å with an rms value of 0.0519 Å. The average Si-Si-Si bond angle is 108.36° with an rms value of 12.35°. The excess energy of the supercell compared to c-Si supercell of the same size is calculated to be 0.23 eV/atom, which is higher than the experimental values, 0.09-0.17 eV/atom. To further decrease the excess energy, we added three Si atoms in their most stable configurations to the supercell, keeping the mass density of the supercell the same as

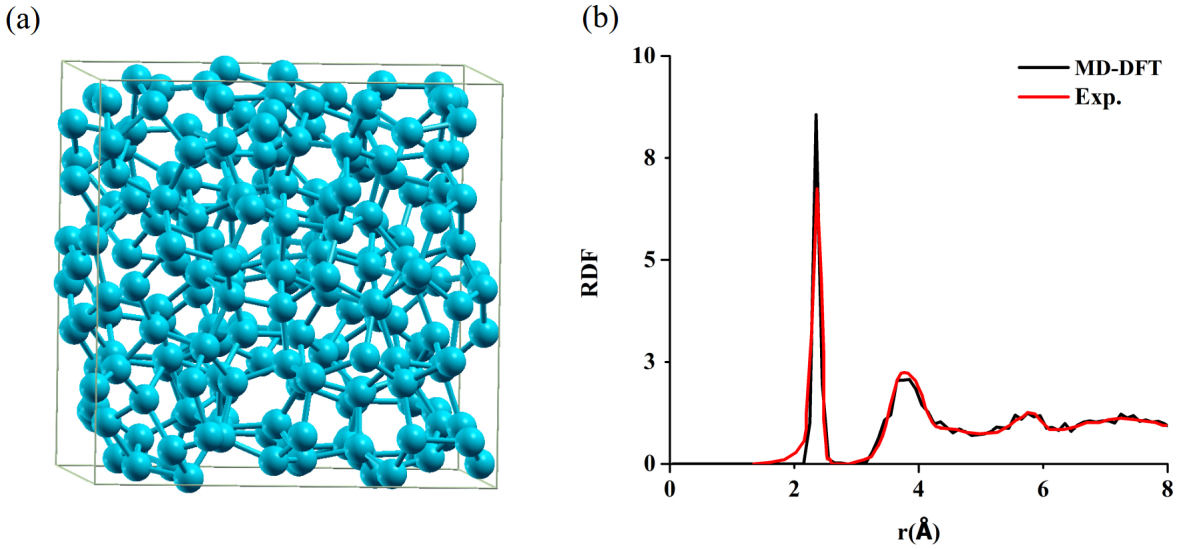

Fig. 1 a) The atomic structure of the a-Si219 supercell and b) the calculated RDF (black lines) of a-Si in comparison with experimental RDF (red lines)[71].

before. The new supercell has four dangling bonds and no floating bonds. The average Si-Si bond length is 2.361 Å with an rms value of 0.0493 Å. The average Si-Si-Si bond angle is 108.47° with an rms value of 11.64° which is very close to the experimental angle distribution of 9-11°. The excess energy of the supercell is 0.19 eV/atom which is close to the upper end of experimental excess energy range (0.09-0.17 eV/atom). The validity of the structures of this supercell was checked by calculating the Radial Distribution Function (RDF) using the LAMMPS program. The RDF gives the probability of finding two atoms in a structure separated by a distance r[70]. Figure 1 shows the calculated RDF of the a-Si structures compared with the experimental results[71]. As can be seen, both the calculated and experimental RDF exhibit a strong peak at 2.3 Å and two weak peaks around 4 and 6 Å.

For obtaining an atomic structural model of a-Si:H with H at%=0.45 (a-Si219H), a single H atom is added to the full relaxed a-Si supercell described in the previous section. Since there are 219 possible sites to bond a hydrogen atom to the supercell corresponding to each of the 219 Si atoms, DFT ion relaxation calculations were carried out on all 219 possible configurations. The configuration with the lowest energy computed by the ion relaxation calculations is chosen as the most stable configuration in order to perform further calculations. The same procedure was repeated for finding the most stable configuration of a-Si:H with H at%=0.9 (a-Si219H2), with the difference being that a single hydrogen atom was added to the most stable configuration of a-Si:H with H at%=0.45. For generating different configurations in this case, the location of the first H atom does not change and only the second H is attached to each of 219 Si atom. The same strategy was used for generating a-Si:H with higher hydrogen concentrations. We finally relaxed all the most stable configurations with the flexible supercell size condition. The vibrational frequencies of the most stable isomers were calculated and no imaginary frequencies were observed, indicating these correspond to a local minima of the structure. We also find the signature the Si-H stretching bond of $\sim$ 2000 cm^{-1} in the calculated vibrational frequencies as another validation of the structures[72]. Here, the short hand label of a-Si219Hn was used to determine the number of H atoms in the supercell where n indicates the number of H atoms in the a-Si supercell containing 219 Si atoms. We also use the label of Si#n to indicate the n^{th} Si atom in the supercell.

Results

Effect of Hydrogen Addition on the Atomic and Electronic Structure of a-Si

As grown, a-Si typically has a high degree of disorder, and contains many undercoordinated Si atoms (dangling bonds), as well as significantly deviated Si-Si bond lengths and Si-Si-Si bond angles compared to bulk crystalline Si (c-Si)[42]. In this section, we first attempt to identify which of the structural defects in a-Si are primarily involved in the addition of H from an energetic standpoint, and second we investigate how the electronic structure changes with this H addition. Towards this goal, we investigate the energy change of a-Si with insertion of hydrogen atoms one by one to the modeled a-Si219 supercell obtained from MD simulation and DFT relaxation calculation.

As mentioned before, we found four dangling bonds (labeled here as Si#1, Si#103, Si#137 and Si#162, illustrated later in Figure 8) in the pure a-Si supercell. Once a H atom is inserted to the supercell, the H atom is traditionally expected to passivate one of these dangling bonds in the most stable configuration of a-Si219H. However, our calculations show that the most stable configuration of a-Si219H corresponds to a H atom bonded to a Si atom (illustrated in Figure 2a) under both bond angle and bond length strain, not to one of the dangling bonds. Bond angle and bond length strain exist when the chemical bonds form under non ideal angles and lengths[73]. The average deviation from the ideal bond angle and bond length involved with the targeted Si atom are 12° and 0.10 Å, respectively. We find that binding the H atom to this Si atom results in removing one of the DBs, which is

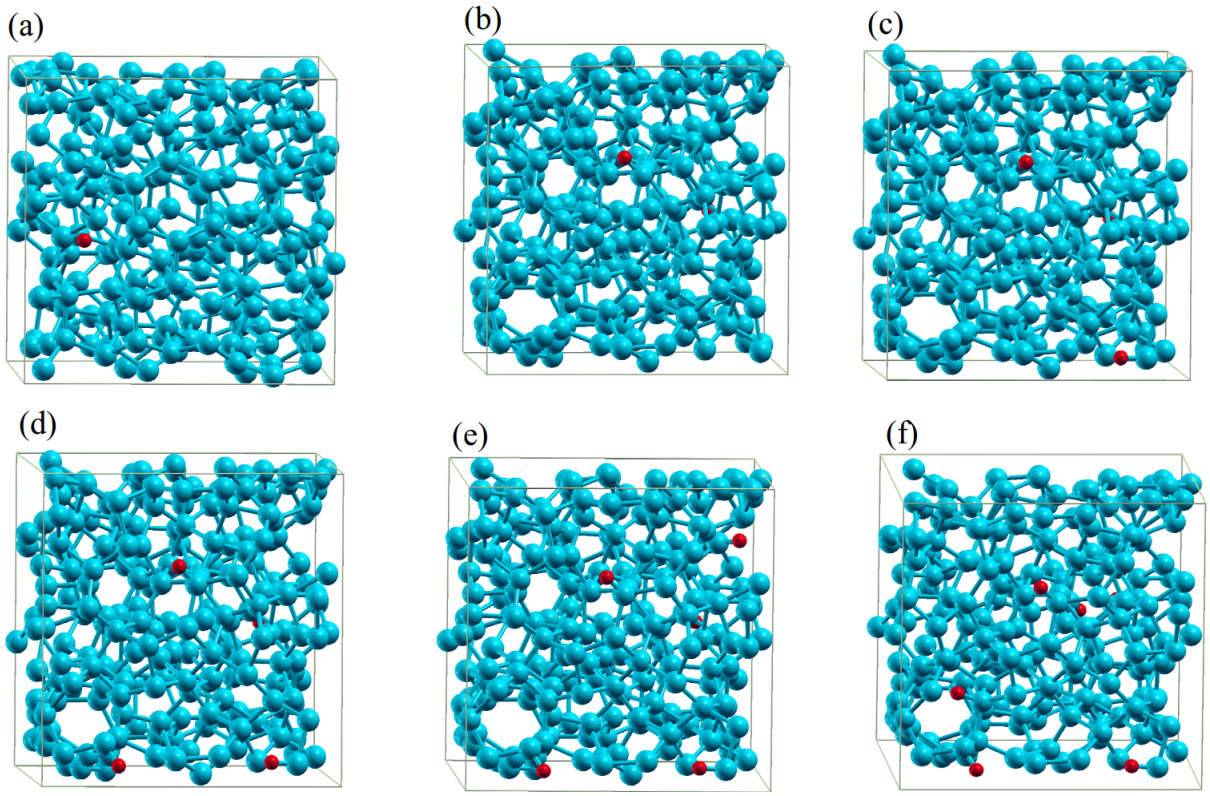

Fig. 2 The position of Si atoms in a-Si structure involved in H addition in a-Si:H with the H atomic percent of a) 0.45% (a-Si219), b) 0.90% (a-Si219H), c) 1.4% (a-Si219H2), d) 1.7% (a-Si219H3), e) 2.2% (a-Si219H4), and f) 2.7% (a-Si219H5).

spatially separated from the H position in the supercell.

As discussed before, we use 2.58 Å as the cutoff bond length for defining a DB. Bonds with any deviation from the ideal bond length (2.35 Å) and ideal bond angle (109.45°) are considered to be strained bonds. Since all the bonds in the a-Si structure are to some degree distorted from an ideal bond in terms of bond length and bond angle with respect to the nearest neighbor atoms, we refer to any bond except those defined as dangling bonds as "strained bonds" in our study.

We observe that the average displacement of Si atoms in the supercells is 0.04 Å, with the maximum of 0.34 Å. This result indicates that H atoms do not simply passivate an isolated dangling bond while the rest of a-Si network is essentially rigid. Rather, in the lowest energy configuration, attaching a H atom to a strained bond is associated with a change in the long range order in the supercell which subsequently results in strain reduction and more stabilization than passivating an isolated dangling bond.

We also examined the atomic structure of a-Si:H, when a second H atom is inserted into the a-Si219H supercell. Our structural analysis shows that, in the most stable configuration, the inserted H atom is bonded to Si#103, which has a dangling bond. By inserting this second H atom to the supercell, two dangling bonds are left in the supercell. The position of this Si atom is depicted in Figure 2b. With continued insertion of H atoms to the supercell, we again find that the highest sensitivity is associated with Si atoms under bond angle or bond length strain to hydrogen addition. Figures 2c, 2d, 2e, and 2f show the Si atoms which in the lowest energy state are involved with H bonding for the third, forth, fifth and sixth H atoms, respectively, added to the supercell. In all these cases, we observe that the number of dangling bonds in the supercell remains the same.

Regarding the hydrogenation energies of the dangling vs strained Si sites, one of the dangling bonds in the supercell (Si#137) is taken as the reference dangling bond. For each H concentration, the energy difference between the hydrogenated strained Si atom and hydrogenated reference dangling bond is calculated and considered as the amount of strain energy released. This amount quantifies the preference for hydrogenation of the strained bonds vs the dangling ones or vice versa. Using this approach, the calculated values are 0.68, 0.46, 0.44, 0.48 eV for a-Si219H, a-Si219H3, a-Si219H4, and a-Si219H6 respectively.

Figure 3 shows a typical histogram of the relative energy of different configurations (here resulting from the addition of one H atom to the a-Si219 supercell). Zero energy corresponds to the most stable configuration. In all the a-Si:H cases studied, the energy difference between the first and second most stable configurations is several kT, and therefore is stable at room temperature. In order to ensure that this energy ordering is not dependent on the DFT method employed, we performed exactly the same DFT simulations as described with the Perdew-Burke-Ernzerhof (PBE) exchange-correlation functional[74,75] on first ten most stable configurations obtained from DFT simulations using the BLYP functional. We find that the most stable configuration remains the same for all H concentrations, and its energy difference with the second most stable configuration still remains several multiples of k_bT at room temperature. Since a-Si:H is usually deposited by

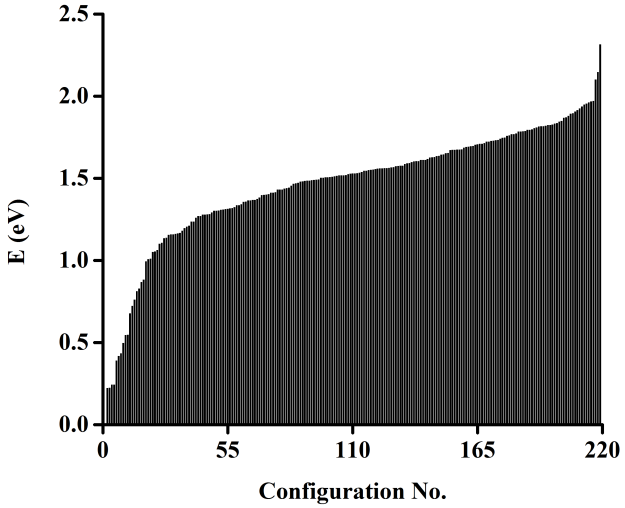

Fig. 3 Histogram of the relative energy of different configurations resulting from the addition of one H atom to the a-Si219 supercell. Zero energy corresponds to the most stable configuration.

plasma deposition under highly non-equilibrium conditions, other less stable configurations should also appear within a particular volume of material[1]. However, these less stable configurations could be converted to more energetically stable ones under appropriate annealing conditions[76].

The details of the electronic properties of a-Si and a-Si:H materials are very important for their application in electronics and optoelectronics. In order to investigate the electronic properties of a-Si and H atom effect, we performed electronic structure calculations on a-Si and on the most stable configurations of a-Si:H. Figure. 4 illustrates the calculated electronic density of states (DOS) plot of the a-Si and a-Si:H valence band compared to photoemission experimental results[77], where a good agreement is observed between experimental and computational results in terms of the height and location of the two characteristic peaks of a-Si and a-Si:H. This agreement provides further evidence (beside the RDF) of the accuracy of the amorphous structure produced by the MD-DFT method.

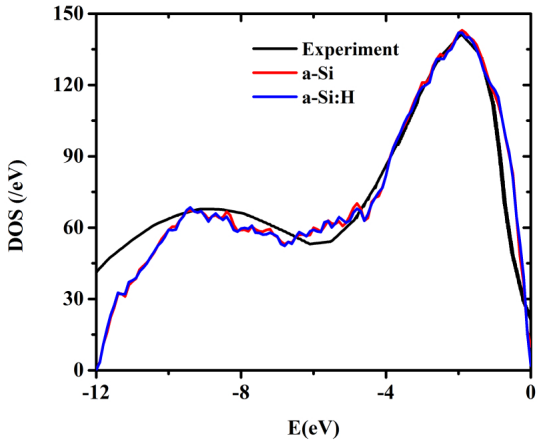

Fig. 4 Calculated DOS of the valence band of a-Si and a-Si:H in comparison with photoemision experiment[77].

From the Figure 4, it is noticeable that the effect of hydrogenation is small on the overall DOS of the valence band of a-Si. However, looking in detail at the DOS close to the valence band edge, it reveals that adding H atoms to the a-Si structure noticeably changes the electronic structure around the band gap. This change mostly includes a decrease in the mid-gap state density, and consequently an increase in the band gap which is in agreement with experimental trends (although the actual Si bandgap is smaller than the experimental value due to well-known issues of conventional DFT). Here, the states inside the band gap of crystalline Si (6.5-7.4 eV) are called midgap states. The decrease in the mid-gap state density with H has been attributed to the passivation of the dangling bonds, the argument being that the insertion of H into a-Si effectively decreases the number of dangling bonds and consequently removes the mid-gap states in the a-Si DOS. However, we find the actual picture is much more complicated. As showed before (Figure 2), in almost all cases H atoms bond to SBs rather DBs, but we still observe midgap state reduction (Figure 5). Particularly, the two dangling bonds in all the a-Si:H supercells remain the same after inserting a third H, however the density of midgap states in the electronic structure of a-Si:H still decreases in H concentration of %2 and %3 (Figure 5). Therefore, we found that the number of dangling bonds in the atomic structure of a-Si and a-Si:H does not necessarily determine the density of midgap states in the electronic structure. Here, the observed mid-gap state reduction can be attributed to increasing structural order of the network through a better annealing processes or H insertion[66]. Increasing the structural order leads to strain release from the whole a-Si structure and leads to the replacement of weak strained Si-Si bonds (which could be the source of midgap states) by strong Si-Si bonds. Another reason for midgap state reduction can be due to the replacement of relatively weak Si-Si bonds by strong Si-H bonds[78]. The formation of strong Si-H bonds results from the interaction of the the shallow orbital of a-Si in the gap or the valence and conduction band edges with H orbitals, which instead create deeper electronic states in the valence and conduction bands. To this end, we believe that the change in excess energy stored in the amorphous network relative to the c-Si gives a better description of the a-Si atomic network than the number of dangling bonds, as proposed in previous studies[67]. Note that we tested different a-Si supercells as a starting atomic structure for the DFT calculations and we obtained consistent results regarding the electronic properties of the a-Si and a-Si:H (SI).

In addition to adding H atoms step by step in their most stable configuration, we looked at the effect of H addition on the DOS when we randomly add H atoms to the a-Si219 supercell rather than their energetically preferred sites. This H addition is more similar to the kinetic conditions encountered experimentally for adding H to a-Si material, e.g. the Plasma Enhanced Chemical Vapor Depositions (PECVD) method. For the random addition of n H atoms to the a-Si219 supercell, n Si atoms are randomly chosen and then a H atom is attached to each of those Si atoms. Finally the structure is fully optimized and its electronic structure is calculated. As seen from Figure 5b, the random addition of H atoms does not significantly decrease the density of midgap states, and

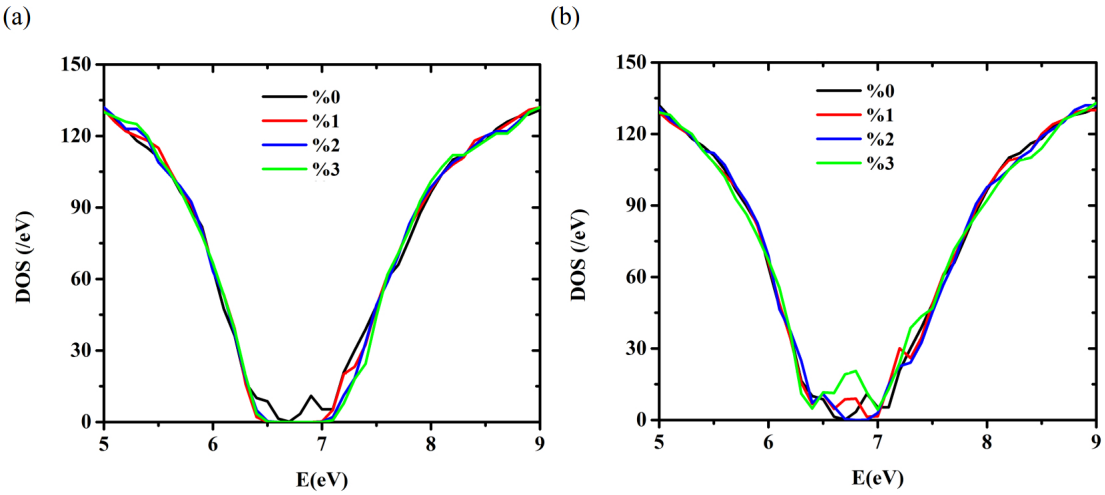

Fig. 5 Calculated DOS of a-Si:H close to the band gap for different H concentrations 0% (a-Si219), 1% (a-Si219H2), 2% (a-Si219H4), and 3% (a-Si219H6) in the case of a) the lowest energy state and b) with H randomly added.

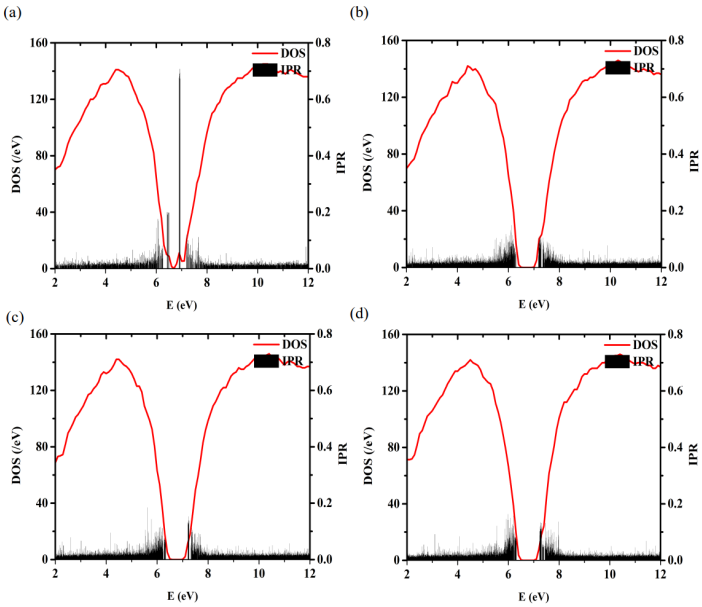

Fig. 6 The calculated IPR of a-Si:H with a) 0% (a-Si219), b) 1% (a-Si219H2), c) 2% (a-Si219H4), d) 3% (a-Si219H6) H atomic concentration.

even in some cases, increases these density of these states. We found that these configurations are less stable than their most stable configurations by 3.16, 3.61, and 8.82 eV for a-Si219H2, a-Si219H4, and a-Si219H6, respectively. The number of DBs in these configurations are 4, 3, and 7 for a-Si219H2, a-Si219H4, and a-Si219H6, respectively. Summarizing, by comparing Figures 5a and 5b, we see that adding H atoms to a-Si under a more thermodynamic reaction control condition leads to better a-Si:H compared to kinetically reaction control condition of H addition. By better quality of a-Si:H, we mean a-Si:H material which contains a lower density of midgap states. A lower midgap state density is usually associated with a lower recombination rate and longer carrier lifetime which generally leads to higher efficiency performance for optoelectronic device applications.

From Figure 5a, we note that the midgap state reduction is fast at lower H concentration, but this change becomes slower at higher H concentration. Therefore, the midgap states density becomes constant and even increases at a certain level of H concentration. This trend implies an optimum value of H concentration in growing a-Si:H material, in good agreement with previous experiments [79].

Localized States Due to Defects and Hydrogen Effect on Orbital Localization

Due to the the presence of structural defects in the atomic structure of an amorphous material, the mobility of holes and electrons in the states close to the valence and conduction band edges are much lower compared to the nonlocalized extended states within the valence and conduction bands, where the carriers are considered free. The energy separation of localized and nonlocalized states is rather sharp and, consequently, this dividing energy is termed the mobility edge [1]. The energy difference between the valence-band mobility edge and conduction-band mobility edge is the so-called mobility gap. Electronic transport in a-Si and a-Si:H is strongly affected by the carriers inside the localized states within the mobility gap. Hence, in this section, we investigate the orbital localization in a-Si and a-Si:H and the structural defects that are responsible for orbital localization in the mobility gap of a-Si and H addition effects on this localization.

The localized properties of an eigenstate can be numerically quantified using the inverse participation ratio (IPR) [80]. The IPR for an eigenstate Ψ_n is given as:

$$IPR(\Psi_n) = \frac{\Sigma_{i=1}^{N} a_{ni}^4}{(\Sigma_{i=1}^{N} a_{ni}^2)^2} \quad (1)$$

where a_{ni} is the coefficient of the i^{th} basis set orbital in the n^{th} Kohn-Sham orbital Ψ_n ($\Psi_n = \Sigma_{i=1}^{N} a_{ni}\phi_i$). The IPR for an ideally extended state is zero, and for an ideally localized state (on one basis orbital) is one. Therefore, higher IPR signifies a higher de-

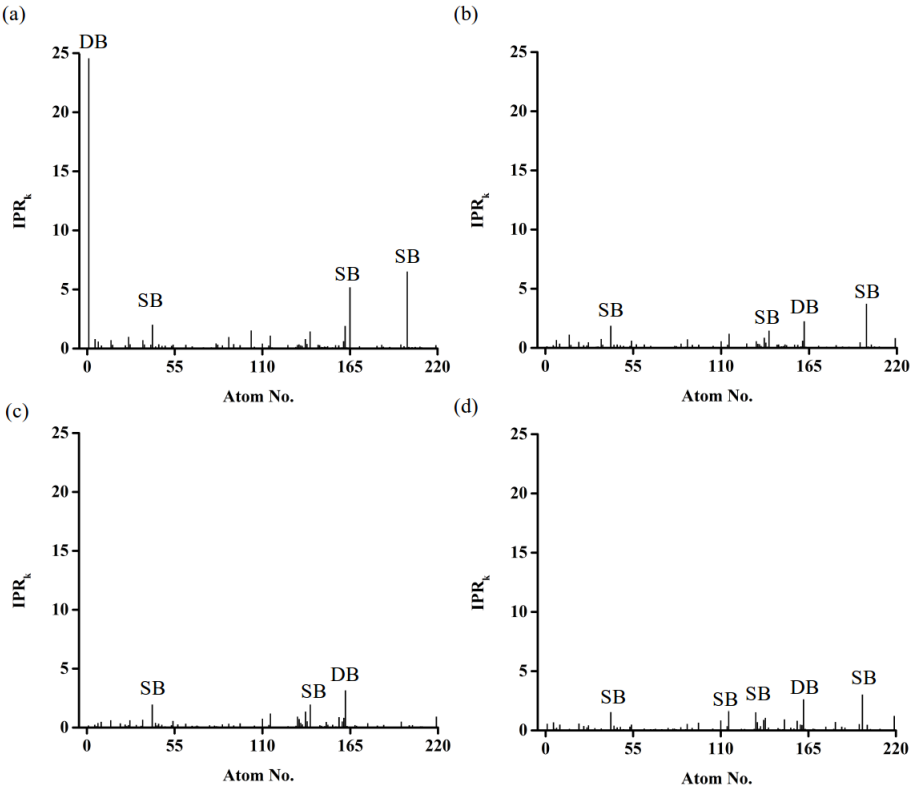

Fig. 7 The relative contribution of each atom in the orbital localization of the modeled a-Si:H supercell with a) 0% (a-Si219), b) 1% (a-Si219H2), c) 2% (a-Si219H4), d) 3% (a-Si219H6) H atomic concentration.

gree of localization. Here, the Kohn-Sham wavefunctions for a-Si structures were obtained using DFT calculations, and in order to quantify the localization properties, the IPR values were computed from Eqn. 1.

Figure 6 shows the calculated IPR of a-Si in comparison with a-Si:H for different H concentrations. As clearly seen, there is a relatively sharp transition between the high and low IPR values (localized and extended electronic states) identifying the existence of the mobility edges in both valence and conduction bands. The general form of the IPR plot is in agreement with previous theoretical and computational studies[42,70]. Here, we consider the mobility gap of a-Si and all a-Si:H structures from 6.0-8.0 eV, since most highly localized states are located in this interval (Figure 6).

From the comparison between the IPR plots presented in Figure 6, we note that the localization of the Kohn-Sham orbitals significantly decreases with the addition of hydrogen atoms. Since H adds primarily to the atoms under bond strain, the decrease in orbital localization is primarily due to removing strained bonds rather than dangling bonds. Localized states strongly influence the effective carrier mobility in terms of scattering centers and hopping conduction[81]. Indeed, in the case of a-Si and a-Si:H, it has been experimentally shown that both the electron and hole mobilities are trapped controlled[82,83]. Therefore a lower degree of localization is consistent with the observation of higher electron and hole mobility in a-Si:H compared to a-Si experimentally[1,17,84]. We note that H atoms change the orbital localization inside the mobility gap much more than outside the mobility gap. This shows that H atoms interact mostly with shallow orbitals close to the valence and conduction band edges of a-Si, and are almost inert to the orbitals far from the valence and conduction band edges.

In order to investigate which structural defects are important in the orbital localization, the contribution of each atom to the localization of all the electronic states in the mobility gap (6.0-8.0 eV) of a-Si was calculated as follows:

$$IPR_k = \Sigma_{n=1}^{N} IPR_{nk}, \tag{2}$$

where N is the total number of electronic states in the mobility gap of a-Si, and IPR_{nk} is the contribution of the k^{th} atom of the system of the orbital localizations of n^{th} Kohn-Sham orbital. The IPR_{nk} can be calculated using the following equation:

$$IPR_{nk} = a_{ni}^4 / (\Sigma_{i=1}^{I} a_{ni}^2)^2, \tag{3}$$

where, as before, a_{ni} is the coefficient of i^{th} basis set orbital coming from the k^{th} atom in the n^{th} Kohn-Sham orbital Ψ_n ($\Psi_n = \Sigma_{i=1}^{N} a_{ni}\phi_i$). Figure 7 shows the IPR_k values for a-Si and a-Si:H with different hydrogen concentration. As seen, there are several strong peaks in the IPR_k graph of a-Si (Figure 7a). Our structural analysis shows that the strongest peak is related to one of the DBs (Si#1) out of four DBs (Si#1, Si#103, and Si#137, Si#162) present in the a-Si219 supercell (Figure 8). This observation is in agreement with the common belief that dangling bonds cause localized states which could trap holes or electrons and act as recombination centers. However one of these four DBs (Si#1) causes much more orbital localization than the other ones.

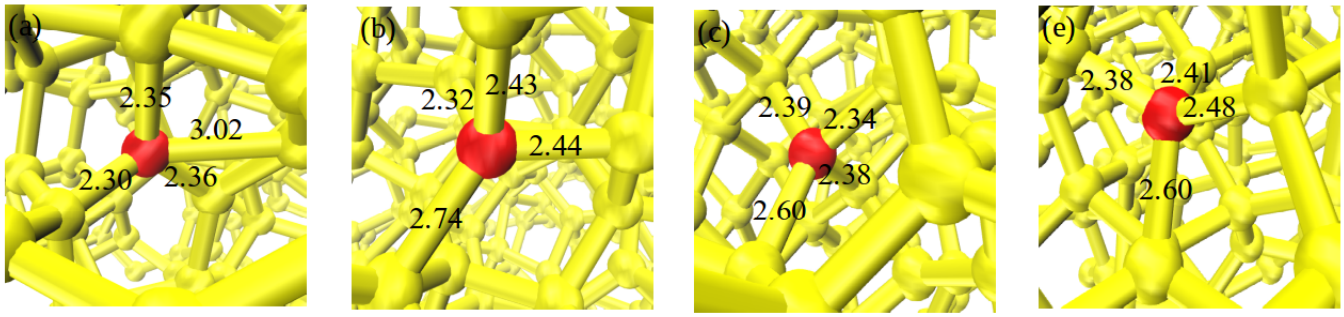

Fig. 8 The position of a) Si#1 b) Si#103 and c) Si#137 atoms d) Si#162 (illustrated with red color) in the a-Si219 supercell and the bond lengths associated with them. All the lengths are in angstroms.

The bond lengths associated with Si#1 are 2.35, 2.30, 2.36, and 3.02 Å (average deviation of 0.18 Å), the bond lengths involved with Si#103 are 2.43, 2.32, 2.44, and 2.74 Å (average deviation of 0.14 Å), the bond lengths associated with Si#137 are 2.39, 2.38, 2.34, and 2.60 Å (average deviation of 0.08 Å), and the bond lengths involved with Si#162 are 2.38, 2.41, 2.48, and 2.60 Å (average deviation of 0.12 Å). Based on the defined cutoff (2.58 Å), all these atoms have one DB, but the length of the bonds which are assigned as DBs are different (Figures 7a and 7b). The length of the DB for Si#1 is longer than the one for the other Si atoms with DBs. Although the assumption is that after a certain bond length cutoff, there is no bond between two Si atoms, but as clearly seen, the shorter DB bond length leads to less orbital localization which could be due to the presence of a relatively weak bond between the two Si atoms connected by a DB. The other strongest peaks in the IPR_k graph of a-Si219 supercell is related to Si atoms under bond strain rather than Si atoms with DBs. Consistent with the a-Si case, strained bonds still create higher or similar localization compared with to dangling bonds in a-Si:H. However, regardless of the H position in the supercell, the contribution of all Si atoms in the orbital localization decreases as the H concentration increases in a-Si:H. As shown before, in almost all the most stable configurations of a-Si:H supercells, H atoms were bonded to Si atoms with strained bonds rather DBs, however this interaction still leads to a reduction in the orbital localization caused by the DBs, over long distances from the H position. This observation provides another indication of the effect of H on long range order in the amorphous structure.

Conclusions

We employed a combined MD-DFT method to obtain stable configurations of a-Si and a-Si:H. Good agreement between the calculated and experimental RDF and DOS is obtained, which demonstrates the validity of our structures for modeling the electronic properties of a-Si and a-Si:H. We found that in almost all the cases, H atoms preferentially bond to Si atoms with strained bonds rather than dangling bonds in the most energetically stable configurations. This H atom interaction with strained bonds is associated with strain release from the amorphous network and leads to a reduction in the midgap states in the electronic structure of a-Si, without passivating dangling bonds. We also found that the Si atoms involved with strained-bonds play a critical role, similar to or even more than that of dangling bonds, in the localization of the orbitals in the mobility gap of a-Si and a-Si:H. The hydrogen atom addition to strained bonds thus strongly decreases the localization of orbitals in the mobility gap and reduce the contribution of all atoms in the orbital localizations.

The primary significance of the results presented here is in demonstrating the importance of reducing the overall strain in the a-Si network through hydrogenation rather than in tying up dangling bonds for improving the quality of a-Si:H material in terms of the density of midgap states. The passivation of dangling bonds is the conventional conceptual picture of the hydrogen passivation process, which the present study shows is far from complete if not misleading. The results are based on lowest energy considerations of where hydrogen bonds, and so represents the thermodynamic limit rather than a kinetically limited hydrogenation process in which H cannot find its lowest energy configuration in the network. Experimentally, a-Si:H is usually deposited using PECVD at relative high pressures of silane and hydrogen gas in a short time period, which corresponds to more kinetically controlled reaction conditions. More thermodynamically controlled conditions during a-Si:H deposition could potentially result in improved passivation at lower H concentrations through control of the growth rates, temperature and post-deposition annealing processes which result in reduced strain in the final material.

Acknowledgements

This material is based upon work primarily supported by the Engineering Research Center Program of the National Science Foundation and the Office of Energy Efficiency and Renewable Energy of the Department of Energy under NSF Cooperative Agreement No. EEC1041895. Any opinions, findings and conclusions or recommendations expressed in this material are those of the author(s) and do not necessarily reflect those of the National Science Foundation or Department of Energy.

Notes and references

1 R. Street, *Technology and applications of amorphous silicon*, Springer Science & Business Media, 2013, vol. 37.

2 M. J. Powell, *IEEE Transactions on Electron Devices*, 1989, **36**, 2753.

3 J. Poortmans and V. Arkhipov, *Thin film solar cells: fabrication, characterization and applications*, John Wiley & Sons, 2006,

vol. 5.
4 L. E. Antonuk, J. M. Boudry, C.-W. Kim, M. Longo, E. Morton, J. Yorkston and R. A. Street, Medical Imaging V: Image Physics, 1991, p. 108.
5 J. Mort, F. Jansen, S. Grammatica, M. Morgan and I. Chen, *Journal of Applied Physics*, 1984, **55**, 3197.
6 D. E. Carlson and C. R. Wronski, *Applied Physics Letters*, 1976, **28**, 671.
7 T. Shimizu, *Japanese Journal of Applied Physics*, 2004, **43**, 3257.
8 E. Stratakis, E. Spanakis, P. Tzanetakis, H. Fritzsche, S. Guha and J. Yang, *Applied Physics Letters*, 2002, **80**, 1734.
9 T. Gotoh, S. Nonomura, M. Nishio, S. Nitta, M. Kondo and A. Matsuda, *Applied Physics Letters*, 1998, **72**, 2978.
10 M. Stutzmann and D. K. Biegelsen, *Physical Review B*, 1989, **40**, 9834.
11 Y. Bar-Yam and J. D. Joannopoulos, *Physical review letters*, 1986, **56**, 2203.
12 R. A. Street, J. Kakalios and T. M. Hayes, *Physical Review B*, 1986, **34**, 3030.
13 Z. E. Smith and S. Wagner, *Physical review letters*, 1987, **59**, 688.
14 H. M. Branz and E. A. Schiff, *Physical Review B*, 1993, **48**, 8667.
15 Y. Pan, F. Inam, M. Zhang and D. A. Drabold, *Physical Review Letters*, 2008, **100**, 206403.
16 L. K. Wagner and J. C. Grossman, *Physical Review Letters*, 2008, **101**, 265501.
17 P. A. Khomyakov, W. Andreoni, N. D. Afify and A. Curioni, *Physical Review Letters*, 2011, **107**, 255502.
18 E. Johlin, L. K. Wagner, T. Buonassisi and J. C. Grossman, *Physical review letters*, 2013, **110**, 146805.
19 T. Mueller, E. Johlin and J. C. Grossman, *Physical Review B*, 2014, **89**, 115202.
20 R. A. Street, J. Kakalios, C. C. Tsai and T. M. Hayes, *Physical Review B*, 1987, **35**, 1316.
21 R. A. Street, M. Hack and W. B. Jackson, *Physical Review B*, 1988, **37**, 4209.
22 R. Biswas, Q. Li, Y. Yoon and H. M. Branz, *Physical Review B*, 1997, **56**, 9197.
23 C. Godet and P. Roca i Cabarrocas, *Journal of applied physics*, 1996, **80**, 97.
24 H. M. Branz, *Physical Review B*, 1999, **60**, 7725.
25 H. M. Branz, *Physical Review B*, 1999, **59**, 5498.
26 S. Sriraman, S. Agarwal, E. S. Aydil and D. Maroudas, *Nature*, 2002, **418**, 62–65.
27 T. A. Abtew and D. A. Drabold, *Physical Review B*, 2006, **74**, 085201.
28 P. A. Fedders, D. A. Drabold and S. Nakhmanson, *Physical Review B*, 1998, **58**, 15624.
29 M. Stutzmann, W. B. Jackson and C. C. Tsai, *Physical Review B*, 1985, **32**, 23.
30 R. Atta-Fynn, P. Biswas *et al.*, *MRS Advances*, 2019, **4**, 87.
31 N. Bernstein, B. Bhattarai, G. Csányi, D. A. Drabold, S. R. Elliott and V. Deringer, *Angewandte Chemie*, 2019, **131**, 7131.
32 V. L. Deringer, N. Bernstein, A. P. Bartók, M. J. Cliffe, R. N. Kerber, L. E. Marbella, C. P. Grey, S. R. Elliott and G. Csányi, *The journal of physical chemistry letters*, 2018, **9**, 2879.
33 D. Igram, B. Bhattarai, P. Biswas and D. A. Drabold, *Journal of Non-Crystalline Solids*, 2018, **492**, 27.
34 A. Pandey, P. Biswas, B. Bhattarai and D. Drabold, *Physical Review B*, 2016, **94**, 235208.
35 Y. Furukawa and Y.-i. Matsushita, *Journal of the Physical Society of Japan*, 2017, **87**, 024701.
36 P. Biswas, D. Paudel, R. Atta-Fynn, D. A. Drabold and S. R. Elliott, *Physical Review Applied*, 2017, **7**, 024013.
37 I. Santos, M. Aboy, L. A. Marqués, P. López and L. Pelaz, *Journal of Non-Crystalline Solids*, 2019, **503**, 20.
38 P. Czaja, U. Aeberhard, M. Celino, S. Giusepponi and M. Gusso, *arXiv preprint arXiv:1703.10487*, 2017.
39 M. Hejna, P. J. Steinhardt and S. Torquato, *Physical Review B*, 2013, **87**, 245204.
40 E. Guerrero and D. A. Strubbe, *Bulletin of the American Physical Society*, 2017.
41 R. Atta-Fynn, D. A. Drabold, S. R. Elliott and P. Biswas, *Physical Review B*, 2017, **95**, 104205.
42 M. Legesse, M. Nolan and G. Fagas, *Journal of Applied Physics*, 2014, **115**, 203711.
43 L. Merid, M. Nolan and G. Fagas, *The Journal of Physical Chemistry C*, 2013, **117**, 23956.
44 T. Vazhappilly and D. A. Micha, *Chemical Physics Letters*, 2013, **570**, 95.
45 C. Freysoldt, G. Pfanner and J. Neugebauer., *Journal of Non-Crystalline Solids*, 2012, **358**, 2063.
46 P. Biswas, D. Drabold and R. Atta-Fynn, *Journal of Applied Physics*, 2014, **116**, 244305.
47 D. Adler, *Solar cells*, 1983, **9**, 133.
48 K. Morigaki, *Japanese journal of applied physics*, 1988, **27**, 163.
49 G. Mueller, *Applied Physics A: Materials Science & Processing*, 1988, **45**, 41.
50 A. Kołodziej, *Opto-electronics review*, 2004, **12**, 21.
51 G. Pfanner, C. Freysoldt, J. Neugebauer, F. Inam, D. Drabold, K. Jarolimek and M. Zeman, *Physical Review B*, 2013, **87**, 125308.
52 I. Kaiser, N. H. Nickel, W. Fuhs and W. Pilz, *Physical Review B*, 1998, **58**, R1718.
53 J. J. Boland and G. N. Parsons, *Science*, 1992, **256**, 1304.
54 N. H. Nickel and W. B. Jackson, *Physical Review B*, 1995, **51**, 4872.
55 H. Shirai, J.-i. Hanna and I. Shimizu, *Japanese journal of applied physics*, 1991, **30**, L679.
56 G. Fugallo and A. Mattoni, *Physical Review B*, 2014, **89**, 045301.
57 I. Solomon, R. Benferhat and H. Tran-Quoc, *Physical Review B*, 1984, **30**, 3422.
58 J. Tersoff, *Physical Review B*, 1989, **39**, 5566.

59 R. Krishnan, J. S. Binkley, R. Seeger and J. A. Pople, *The Journal of Chemical Physics*, 1980, **72**, 650.

60 P. Giannozzi, S. Baroni, N. Bonini, M. Calandra, R. Car, C. Cavazzoni, D. Ceresoli, G. L. Chiarotti, M. Cococcioni, I. Dabo *et al.*, *Journal of Physics: Condensed Matter*, 2009, **21**, 395502.

61 S. Le Roux and V. Petkov, *Journal of Applied Crystallography*, 2010, **43**, 181.

62 A. D. Becke, *The Journal of Chemical Physics*, 1993, **98**, 5648.

63 C. Lee, W. Yang and R. G. Parr, *Physical Review B*, 1988, **37**, 785.

64 M. Ishimaru, S. Munetoh and T. Motooka, *Physical Review B*, 1997, **56**, 15133.

65 I. Štich, R. Car and M. Parrinello, *Physical Review B*, 1991, **44**, 11092.

66 M. Nolan, M. Legesse and G. Fagas, *Physical Chemistry Chemical Physics*, 2012, **14**, 15173.

67 A. Pedersen, L. Pizzagalli and H. Jónsson, *New J. Phys*, 2017, **19**, 063018.

68 J. Custer, M. O. Thompson, D. Jacobson, J. Poate, S. Roorda, W. Sinke and F. Spaepen, *Applied Physics Letters*, 1994, **64**, 437.

69 A. Smets, W. Kessels and M. Van de Sanden, *Applied physics letters*, 2003, **82**, 1547.

70 K. Jarolimek, R. A. deGroot, G. A. deWijs and M. Zeman, *Physical Review B*, 2009, **79**, 155206.

71 K. Laaziri, S. Kycia, S. Roorda, M. Chicoine, J. L. Robertson, J. Wang and S. C. Moss, *Physical Review Letters*, 1999, **82**, 3460.

72 F. Gaspari, I. Kupchak, A. Shkrebtii and J. Perz, *Physical Review B*, 2009, **79**, 224203.

73 J. March, *Advanced organic chemistry: reactions, mechanisms, and structure*, John Wiley & Sons, 1992.

74 J. P. Perdew, K. Burke and M. Ernzerhof, *Physical review letters*, 1996, **77**, 3865.

75 W. Lei, D. Liu, X. Chen, P. Zhu, Q. Cui and G. Zou, *The Journal of Physical Chemistry C*, 2010, **114**, 15574.

76 I. Kwon, R. Biswas and C. M. Soukoulis, *Physical Review B*, 1992, **45**, 3332.

77 J. Singh, *Physical Review B*, 1981, **23**, 4156.

78 J. Nelson, *The physics of solar cells*, World Scientific Publishing Co Inc, 2003.

79 G. D. Cody, T. Tiedje, B. Abeles, B. Brooks and Y. Goldstein, *Physical Review Letters*, 1981, **47**, 1480.

80 J. Dong and D. A. Drabold, *Physical Review Letters*, 1998, **80**, 1928.

81 N. W. Ashcroft and N. D. Mermin, *Solid state physics*, Holt, Rinehart and Winston, 1976.

82 A. Moore, *Applied Physics Letters*, 1977, **31**, 762.

83 J. Marshall, R. Street and M. Thompson, *Philosophical magazine B*, 1986, **54**, 51.

84 Y. Hayashi, D. Li, A. Ogura and Y. Ohshita, *IEEE Journal of Photovoltaics*, 2013, **3**, 1149.

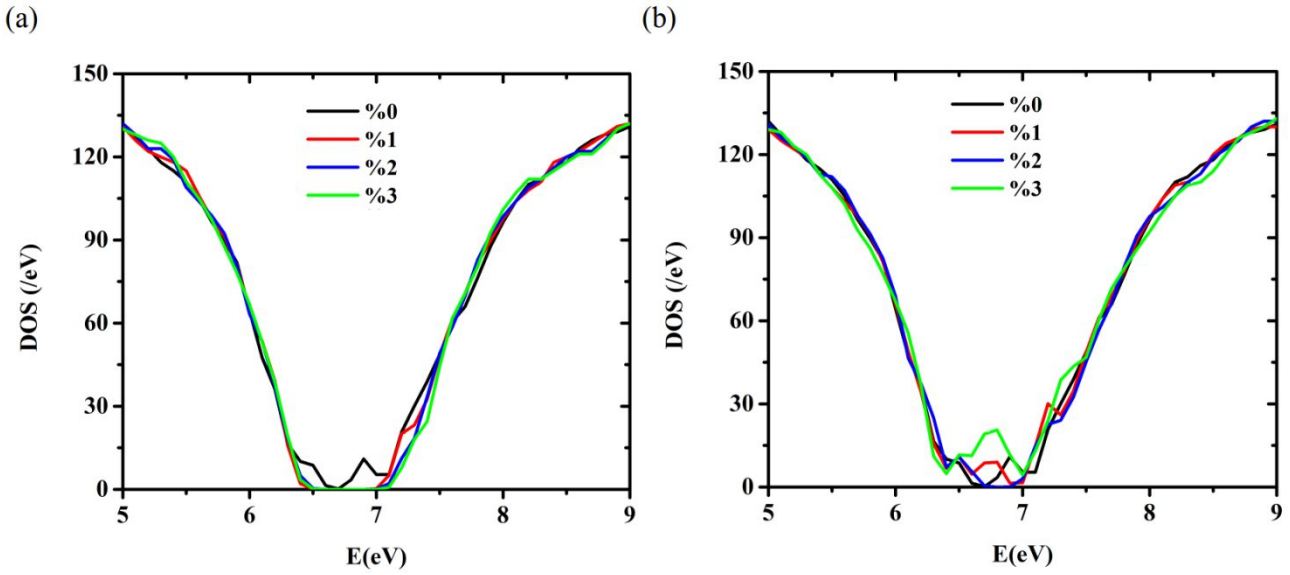

Calculated DOS of a-Si:H close to the band gap for different H concentrations in the case of a) thermodynamically b) kinetically H addition.